Measurement of Particle Size Distribution of Tripalmitin Crystals in a Model Solution Using a Laser Diffraction Method

Andrea M. Fitzgerald[a], O. John Barnes[b], Ian Smart[b], and D. Ian Wilson[a,*]

[a]Department of Chemical Engineering, University of Cambridge, Cambridge, CB2 3RA, United Kingdom, and [b]United Biscuits Group R&D, High Wycombe, HP12 4JX, United Kingdom

ABSTRACT: The form and size distribution of tripalmitin (PPP) crystals formed by quenching a solution in a batch crystallizer have been studied using scanning electron microscopy and a laser diffraction technique. Although the accuracy of the laser technique for particle sizing was affected by the nonsphericity of the crystals, the technique proved to be effective and very reproducible. Crystals recovered by filtration and sonication for laser sizing exhibited markedly different particle size distributions (PSD) and shapes compared to those prepared using another standard route, namely, suspension in butanol and centrifugation. Solutions of 2–10 wt% PPP in a paraffin solvent were crystallized at 25–40°C and displayed two ranges of behavior: (i) rapid growth under strongly supersaturated conditions, yielding narrow PSD of plate and needle-like crystals; and (ii) slow growth in the metastable regime, yielding spherulitic aggregates of platelets that broke down under sonication during preparation for laser sizing. Suspension in alcohol followed by centrifugation yielded aggregates that did not break down under sonication, indicating that the sample preparation route affected the result of the analysis.

Paper no. J9924 in *JAOCS 78,* 1013–1020 (October 2001).

KEY WORDS: Crystallization, particle size distribution (PSD), tripalmitin.

The crystallization behaviors of palm oil and palm olein, the liquid fraction of palm oil, have been studied at length. Palm oil is a complex natural product, composed of more than 12 triglycerides that make up as much as 94% by weight of the oil. In addition, it also contains up to 5% diglycerides (1). Tripalmitin (PPP), present in significant quantities in palm oil, has long been associated with the unwanted formation of crystals and subsequent clouding of palm olein (2,3). In food-processing industries, palm oil blends are frequently mixed with other ingredients and partially crystallized to give a plasticized fat. However, during subsequent transport of the crystallized oil blend, deposition of PPP and other fats can occur onto the wall of delivery pipelines, a phenomenon known as "coring." Depositions of this type in process equipment can lead to increased maintenance, cleaning, and fuel costs (4) and also to more severe concerns related to hygiene, which are of prime importance in food processing (5). Analogous situations exist in the oil industry, where the formation of wax can be a major problem in oil well tubing and submarine pipelines (6), and models have been developed to predict and circumvent the buildup of unwanted deposits (7).

The quality of plasticized fat is related both to the extent of crystallization and the size of crystals present in the suspension. In the food fat coring scenario, particle size distributions (PSD) are particularly important because the mode of particle transport to the wall and subsequent adhesion are strongly related to particle size and shape. Information on particle size and shape is required to identify and model the mechanisms involved in deposition (e.g., Ref. 8). Previous studies have focused on measurement of PPP crystal size by optical methods (9). Although laser diffraction has been utilized to study the crystal size of shortenings (10) directly suspended in isobutanol, this technique is not suitable where a fat solution forms emulsions with alcohols. In this paper, we describe a simple method for measuring PPP crystal size using a laser diffraction–based method so that statistically representative distributions are obtained. This work represents part of an investigation of the coring phenomenon based on model solutions of PPP in a noncrystallizing solvent, here a paraffin blend (11). Previous studies of crystallization behavior of PPP from the melt (12) and from triolein solutions (13) have paid particular attention to crystal morphology and transformations between α, β', and β polymorphs. Polymorphism was not studied in detail in this study, partly because previous work in the area, on crystallizing triglycerides in nonsimilar solvents (14), stated that in these systems the crystals are in the most stable modification and there are no mixed crystals, and partly because the focus in this work was on meso- and macrostructure features, manifested in PSD, rather than on crystal order.

EXPERIMENTAL PROCEDURES

Materials. Heavy liquid paraffin ($\rho_{25°C}$ = 0.773 g/cm^3; $\eta_{25°C}$ = 280 mPa·s) was obtained from BDH Chemical (Poole, United Kingdom). PPP (>95% purity) was obtained from Sigma-Aldrich (Poole, United Kingdom). Solvents used were of a standard laboratory grade.

Crystallization of samples. PPP solutions in paraffin were prepared at concentrations of 2, 5, and 10 wt%. Solutions were held at 70°C for at least 30 min prior to crystallization to erase any thermal history. One liter of the hot solution was introduced into a stirred (400 rpm; RZR 2050 stirrer, Heidolph, Kelheim,

*To whom correspondence should be addressed at Department of Chemical Engineering, University of Cambridge, Pembroke Street, Cambridge, CB2 3RA, United Kingdom. E-mail: ian_wilson@cheng.cam.ac.uk

Germany), jacketed glass crystallization vessel maintained at the required temperature by circulation of water through the jacket using a C10-K15 circulator (Gebr. Haake GmbH, Karlsruhe, Germany). Temperatures were measured using platinum resistance thermometers (±0.2 K; Lab Facility, Hampton, Middlesex, United Kingdom) and recorded by a personal computer datalogger. The cooling rate was determined by the temperatures used in experiments; the initial cooling rates in the experiments reported here were in the order of 1–2 K/min.

Preparation of crystal samples by filtration. All samples were prepared by this method, with the exception of those where direct comparisons were sought between this method and separation by centrifugation. Aliquots (5 mL) of the crystallizing solution were removed from the crystallizer at 10 min intervals and filtered under vacuum through a 0.2 μm nylon membrane filter paper (Whatman, Maidstone, United Kingdom). The filtered solids were first washed with hexane (at ambient temperature) to remove any entrained paraffin and then with acetone to remove any remaining hexane, and finally dried overnight. The filtration stage was completed in approximately 5 min.

Preparation of samples by centrifugation. Aliquots (10 mL) of the crystallizing solution were removed from the crystallizer as described above, suspended in 50 mL of isobutanol, and shaken thoroughly, creating an emulsified suspension. This suspension was centrifuged for 30 min at $2200 \times g$. The upper liquid portion was discarded, and another 50 mL of butanol added to wash the solution. This was then recentrifuged, under identical conditions. Finally the sample was washed with acetone, centrifuged to remove any entrained butanol, and dried at room temperature. The centrifugation stages took approximately 90 min to complete. There were noticeable difficulties in maintaining a constant solution temperature in the centrifuge.

Preparation of samples for particle size analysis. Isopropanol was filtered through a 0.1 μm cellulose nitrate membrane filter paper (Whatman) to remove any dust and particulate matter. A small amount of the filtered solids (approximately 20 mg) was added to approximately 2 mL of filtered isopropanol. The solution was then sonicated in an ultrasonic bath (Lucas Dawes, London, United Kingdom) to give a uniform suspension of PPP crystals.

Particle size analysis methods. A microvolume module (capacity 15 mL) for a particle size analyzer (Coulter LS230; Beckman Coulter, High Wycombe, United Kingdom; particle size analysis range 0.04–2000 μm) was filled with approximately 12 mL of filtered isopropanol and placed inside the instrument. The laser was aligned and a background reading taken according to the manufacturer's instructions. Small amounts of the sonicated sample were added stepwise to the microvolume module until the suspension of crystals gave a reliable measurement. Three consecutive analyses of particle size distribution were performed, lasting 1 min each with a 30 s interval between measurements. The amount of sample suspended in solution in the microvolume module was checked throughout a run, and a small amount of sample was added in the interim 30 s period if it appeared to be falling too low. After analysis of each sample, the cell was thoroughly rinsed with isopropanol, refilled, and placed back in the instrument. The laser was then realigned, a new background reading taken, and the analysis performed for the next sample. All PSD reported here are expressed as a percentage volume differential, and the mean diameters quoted are calculated as a volume weighted mean diameter, commonly referred to as D(4,3) or d_{43} (Eq. 1).

$$d_{43} = \sum_{c=1}^{N} n_c d_c^4 \Big/ \sum_{c=1}^{N} n_c d_c^3 \qquad [1]$$

where d_c denotes the diameter of a particle allocated to the cth sampling interval in the instrument spectrum and n_c is the number fraction of particles in the cth interval. Thus, for a monodispersed sample, d_{43} is the common diameter. The instrument calculates the number fraction in each interval, using an inverse algorithm by comparing the observed diffraction/scattering behavior with that predicted using a numerical model.

The authors also tried, without success, to use an electrozone device (or "Coulter counter"; Elzone PC240, Particle Data Systems, Luxembourg) to study these PSD. This technique yields true concentrations and a particle size based on particle volume rather than scattering area, but requires a conductive liquid phase. Comparison of the PSD generated by the different methods would have provided further insight into shape and the like. However, finding either an organic solvent or solution that was sufficiently conductive or an ionic solution that did not cause the crystals to congeal proved difficult.

Scanning electron microscopy (SEM). Samples of PPP crystals were sputtered with gold for 3 min under vacuum (Emitech K550 sputterer; Ashford, United Kingdom). The samples were then analyzed using a JEOL JSM 820 SEM (JEOL UK Ltd., Welwyn Garden City, United Kingdom). The detector was used in the SEI mode, with a working distance of 10 and an accelerating voltage of 5 kV. Preparation was performed at room temperature and analyses were performed at periods ranging from 1 wk to 1 mon after the original experiments. Samples were stored in the dried, solid form before SEM analysis.

RESULTS AND DISCUSSION

Effect of temperature and concentration on crystallization rate and induction period. Figure 1 shows sets of temperature and mass yield data obtained from crystallization experiments using different PPP concentrations at a target temperature of *ca*. 30°C. The temperature profiles for 5 and 10 wt% show decays caused by heat transfer through the crystallizer walls, followed by a temperature rise as nucleation and growth released the latent heat of crystallization into the solution. The final temperature reached in the crystallizer was normally 2–3 K higher than the initial coolant temperature and remained stable at this level (±0.25 K) for the remainder of the experiment. This temperature transient, namely, the departure from a steady, asymptotic cooling curve, was found to correlate quite reproducibly with the end of the induction period and end of the growth period, and was therefore used to estimate

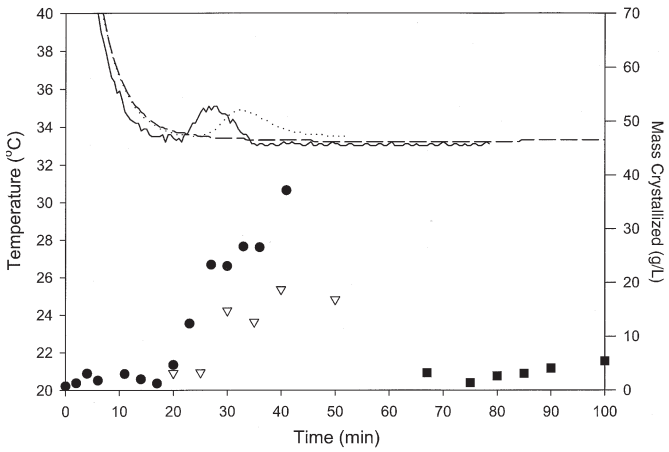

FIG. 1. Crystallizer temperature profiles and mass crystallized at different concentrations of tripalmitin. Initial coolant temperature = 30°C; initial solution temperature = 70°C. ●, —: 10 wt%; ▽, ·····: 5 wt%; ■, - – – –: 2 wt%.

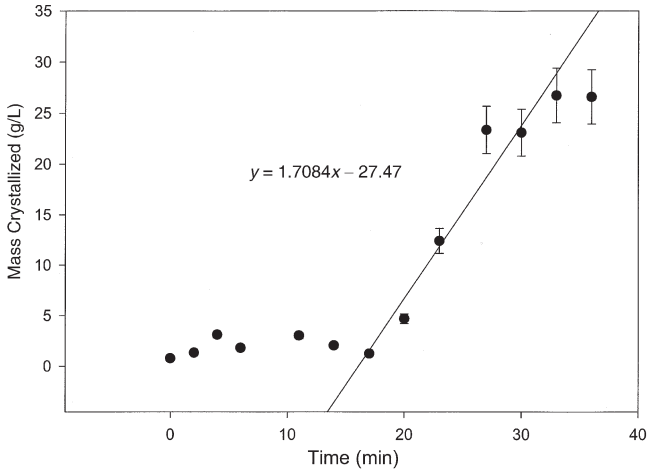

FIG. 2. Mass crystallized over time, with sample fit for crystallization rate determination. Conditions: 10 wt% tripalmitin; coolant temperature = 30°C. Bars indicate spread of values for each data point. Bars do not appear on earlier data points because variation was small and within the size of the symbols used.

the time co-ordinate in determining crystallization rates and induction periods. Moreover, a quantitative analysis of the enthalpy associated with the temperature peaks gave very good agreement with the enthalpy change expected for the yield of crystals (calculated using $\Delta H_{freezing}$ = 147 kJ/mol, measured by differential scanning calorimetry; 15).

The temperature–time profiles obtained showed a distinct difference in induction times and crystallization rates with concentration at the same target temperature and initial cooling rate (~1 K/min). Figure 1 shows that the 5 wt% solution crystallized slightly later than the 10 wt% case, whereas the 2 wt% solution crystallized significantly later, with a barely discernible evolution of crystallization enthalpy, indicating a slow reaction. These results are consistent with the 10 and 5 wt% solutions being significantly oversaturated at ~30°C (saturation temperatures 51 and 44°C, respectively), whereas the 2 wt% solution (saturation temperature 41°C) shows the longest induction period, as expected for homogeneous nucleation under metastable conditions. Temperature and mass profiles obtained at other bulk temperatures showed similar trends (data not reported).

The mass yield measurements could not be performed very rapidly, and the scatter in the data (see Fig. 2) also precluded the use of more detailed kinetic analysis such as the Avrami equation. Linear rates were therefore extracted from the mass yield profiles, as shown in Figure 2. Care was taken to ensure that the data points used for regression lay within the bounds indicated by the thermal measurements. The rate data are summarized in Figure 3. This figure shows that the 10 wt% solutions crystallized at approximately the same rate (2 g/L min) within experimental error over this range. The 5 wt% solutions also exhibited uniform rates of crystallization (1 g/L min) at lower temperatures, but the rate dropped noticeably above 35°C, which is attributed to the system entering the metastable regime. The rate for the 2 wt% crystallizations was uniformly low; the laboratory configuration used here did not permit studies at temperatures much below 25°C, where the 2 wt% solution would have been strongly supersaturated. These observations indicate that, for higher concentrations at lower temperatures, crystallization was predominantly mass transfer–controlled, although it is possible that this was also linked to viscosity effects (16). Kinetic effects arise at higher temperatures and lower concentrations, when the solution lies in the metastable region.

The induction period for crystallization was defined as the time at which the crystallized mass started to increase markedly. Note that this time includes the time taken for the temperature in the crystallizer to reach the target temperature (approximately 16 min in Fig. 1). For the example in Figure 2, the end of the induction period was taken to be 20 min. The induction period data are summarized in Figure 4. The 5 and 10 wt% data, corresponding to rapid growth conditions in Figure 3, exhibit very similar induction periods, which increased in a quasi-linear fashion with temperature. The larger induction periods observed for 5 wt% solutions at temperatures >36°C correspond to the kinetic control conditions in Figure 3 and the approach of the metastable region. The larger

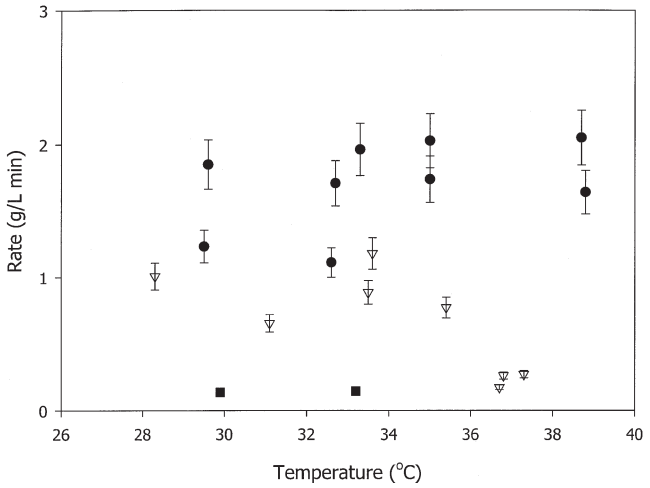

FIG. 3. Effect of temperature on crystallization rate. ●, 10 wt%; ▽, 5 wt%; ■, 2 wt%. Bars indicate spread of values for each data point.

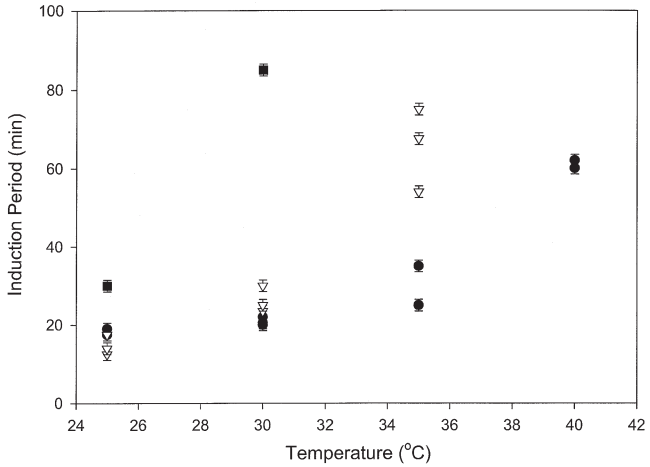

FIG. 4. Variation of induction period of crystallization with temperature and concentration.●, 10 wt%; ▽, 5 wt%; ■, 2 wt%. Error bars indicate spread of values associated with each data point.

induction period for the 10 wt% tests at 39°C was not accompanied by a reduction in rate, but the induction period was still significantly smaller than would be expected for 5 wt% at 39–40°C (4 K subcooling). The 2 wt% data show similar trends, with induction periods of 86 min for 8 K subcooling, and 29 min for 11 K subcooling. The effects of formation kinetics on PSD are discussed below.

Effect of sonication time on PSD. A sample obtained from crystallization of a 10 wt% solution at 30°C was used to evaluate the effect of sonication time on PSD in order to establish an optimal or threshold period. Figure 5 shows the PSD after sonication times of 2–5 min. No measurements were made at shorter periods as the number of crystals in suspension were too few to allow measurement. The figure shows that more large particles were found after prolonged sonication; this was because the smaller particles were the first to be suspended and are therefore most evident in the initial stages. On further sonication, larger particles became fully suspended, correlating with the visual observation of all the solid material being in suspension. The d_{43} mean values increased with time, from 4.3 μm (mode 3.9 μm) at 2 min to 5.0 μm (mode 4.3 μm) at 5 min. It can be seen that no change in PSD is evident after 4 min, so a 5 min period was selected for sonicating samples to ensure that all solids were suspended. This period was used in all subsequent measurements.

Variation of PSD with time between measurements. Three measurements of PSD were performed on the same sample, with a 1 min interval between each. There was little visible difference between the PSD, and a statistical analysis indicated minimal fluctuation in the distributions, with the mean particle size varying by only 0.25 μm, which is comparable to the accuracy of the laser scattering technique.

Reproducibility of crystallization protocols. The results from two samples crystallized in different batches under identical conditions yielded virtually identical PSD, with the shape of the distribution being the same and the mean particle diameter differing by only 0.06 μm. This confirmed that both the crystallization procedure and PSD method were reproducible. The rate and induction period data shown in Figures 3 and 4 exhibited noticeably greater scatter, which is related to the difficulty in controlling homogeneous nucleation rates.

Effect of crystallization time on PSD. A 10 wt% solution was crystallized at 35°C and samples removed from the crystallization vessel at regular intervals while crystallization was occurring. A final sample was obtained after leaving the crystallized solution stirring until 18 h had elapsed. The PSD of the sample obtained varied little in shape and mean diameter, the latter being 6.0, 6.1, and 5.7 μm for samples obtained after 35 and 45 min and 18 h, respectively. All the other samples studied showed similar results with there being no significant

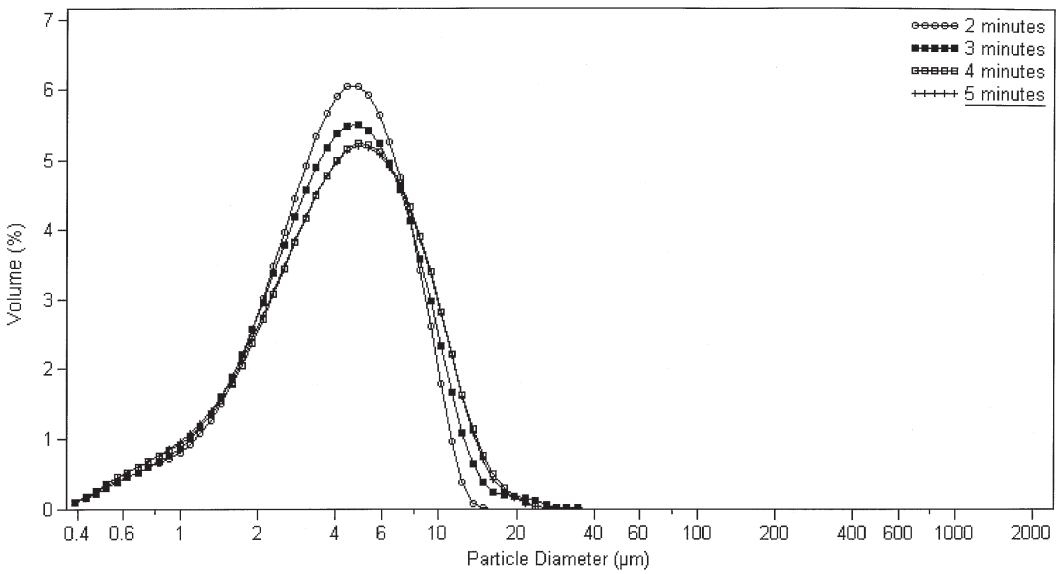

FIG. 5. Particle size distributions of a 10 wt% sample crystallized at 30°C after sonication for 2, 3, 4, and 5 min, respectively.

TABLE 1
Effect of Concentration and Temperature on Particle Size Distribution

Crystallization temperature (°C)	Size (μm)	PPP concentration[a]		
		10 wt%	5 wt%	2 wt%
40	Median	3.3	4.1	10.7
	d_{43}	3.7	4.5	10.9
	Mode	4.0	4.4	12.4
35	Median	5.2	9.1	—
	d_{43}	5.7	9.8	—
	Mode	6.1	11.3	—
40	Median	7.5	15.9	—
	d_{43}	8.0	16.6	—
	Mode	9.4	21.7	—

[a]PPP, tripalmitin.

variation of the PSD during the course of a crystallization experiment. This feature will considerably simplify the understanding and modeling of deposition behavior under these types of conditions.

Effect of concentration and temperature on PSD. Table 1 shows the relationship between concentration, crystallization temperature, and mean particle size. It is evident that particle sizes (mean and mode) increased noticeably with increase in temperature. The trend is more striking for the 5 wt% studies, with an order of magnitude change in d_{43} over the 10 K change in temperature and transition into the metastable region. The distributions featured similar patterns, namely, a broad peak with a significant proportion of smaller crystal sizes (especially when number fraction, rather than volume fraction, is considered). The PSD for 10 wt% PPP at 30°C (Fig. 6) featured a shoulder in the distribution around 1 μm, indicating a possibly bimodal distribution. Further work is under way to ascertain whether polymorphism is responsible for this shoulder, which was not observed at other concentrations and temperatures.

The effect of concentration on PSD at 30°C is evident in Figure 6. The modal particle size for the 2 wt% solution, at ~12 μm (d_{43} = 10.9 μm), was significantly greater than those observed at 5 and 10 wt%. These variations in particle sizes are most likely a direct consequence of the different kinetics observed in the nucleation and growth of the crystals. Figures 3 and 4 show that, over the temperature range considered here (29–40°C), the induction periods and mass crystallization rates for the 10 wt% runs were similar. The corresponding values of d_{43} are similar and increase with temperature, reflecting the importance of growth over nucleation as supersaturation decreases. The very noticeable differences in PSD correlate with noticeable variation in induction times and mass growth rates in Figures 4 and 3, respectively. At the higher temperatures, the nucleation rate is significantly reduced (hence longer induction period); growth becomes more pronounced, and the PSD is shifted toward the right. For the 2 wt% solutions, Figure 4 indicates that the induction time for the 2 wt% solution was 50% longer than those observed at higher concentrations, while Figure 3 indicates that the mass growth rate was low: These observations are consistent with a reduced nucleation rate and hence larger particle sizes.

At low supersaturations, a metastable region has been identified wherein crystals have time to grow to large sizes and associate to form large particulates. At high supersaturation, nucleation-dominated crystallization occurs, yielding small, nonspherical particles. This result has two consequences for the present issue, that is, of deposition on fat surfaces. First, if the individual tri- (and di-) glycerides in a palm oil mixture crystallize out as chemically individual solids, as opposed to a solid solution, a range of supersaturations will exist at any one temperature and thus the plasticized fat will contain a mixture of platelets and spherulites. Second, from the modeling perspective, if conditions promote the formation of spherulites, deposition on a surface can be analyzed

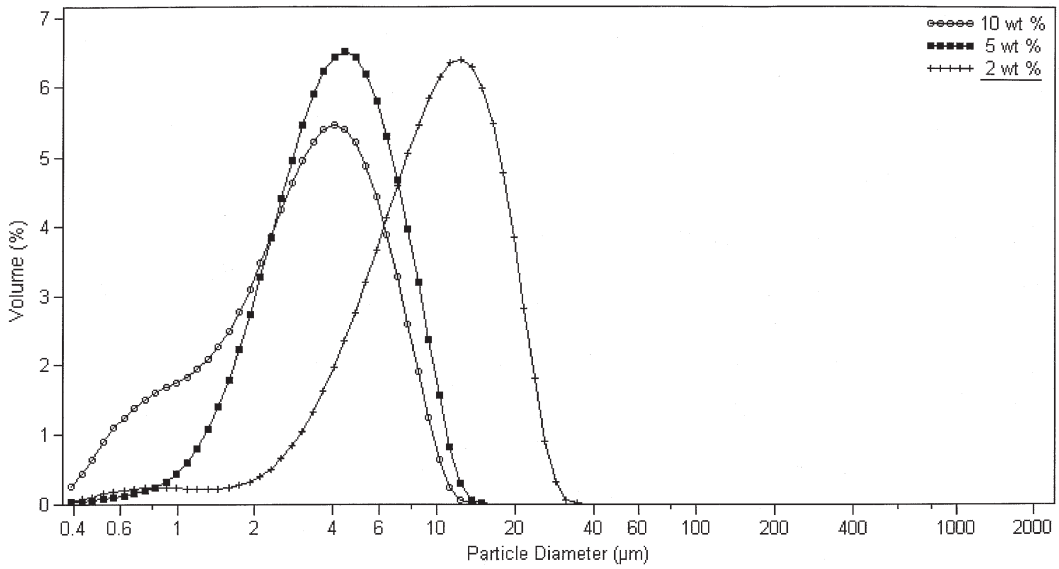

FIG. 6. Particle size distributions of 10, 5 and 2 wt% solutions crystallized at 30°C.

using existing particulate fouling models (e.g., Ref. 8), which are usually based on spherical depositing species. Where platelets dominate the solid structures, more specialized deposition modeling may be required.

Comparison of PSD with SEM images. A comparison of the laser sizing technique with microscopy methods was undertaken, since many of the previous studies of PPP crystallization have employed such methods. Figure 7A shows an SEM micrograph taken of a sample of 10 wt% solution crystallized at 30°C exhibiting needle-form crystals. Visual inspection suggests crystals varying in length from about 3–6+ μm, width 1–3 μm, and thickness <1 μm, which are consistent with the PSD reported in Figure 5. The highly nonspherical shapes evident in the figure assist the interpretation of the PSD in Figure 5: The processing algorithm used to generate the distribution assumes some degree of sphericity, so the mean diameter is not expected to be very reliable. Furthermore, the significant fraction of small crystals is likely owing to scattering by needles aligned with the laser, presenting the smallest dimension, the edge, to the beam. Micrographs of crystals obtained from 5 wt% solutions at 30°C showed very similar features to that in Figure 7A, namely, needles with lengths and widths in the range 2–6 μm, in agreement with the PSD in Table 1.

The micrographs in Figures 7B and 7C of the crystals obtained from 2 wt% solution at 30°C display markedly different spherulitic forms ranging in size from 10 to 100 μm. These spherulite assemblies are not evident in the PSD results (e.g., Fig. 6), which showed a modal size range that corresponded quite closely with the dimensions of the individual platelets (Fig. 7C). Spherulite structures were also observed in micrographs of the 5 wt% samples crystallized at 35°C and above (Fig. 7D), but not in the corresponding PSD. This suggests that these spherulites, being agglomerates, are readily broken down by the forces imposed on them during the sonication conditioning process. Other results confirmed that

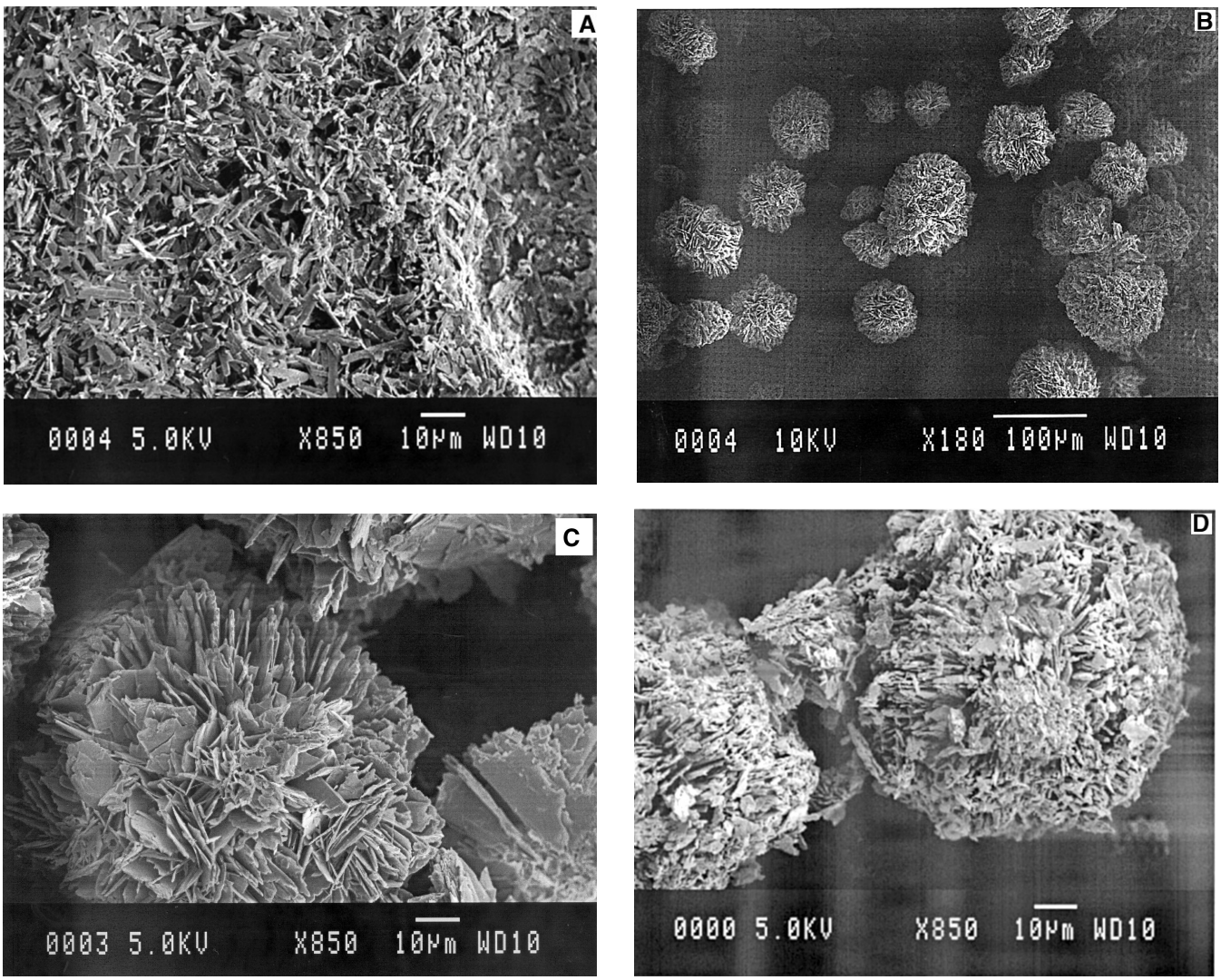

FIG. 7. Scanning electron microscope (SEM) images of tripalmitin crystals recovered by the filtration technique (A) 10 wt% crystallized at 30°C; (B) 2 wt% crystallized at 30°C; (C) close-up of an individual spherulite from B; (D) 5 wt% crystallized at 35°C.

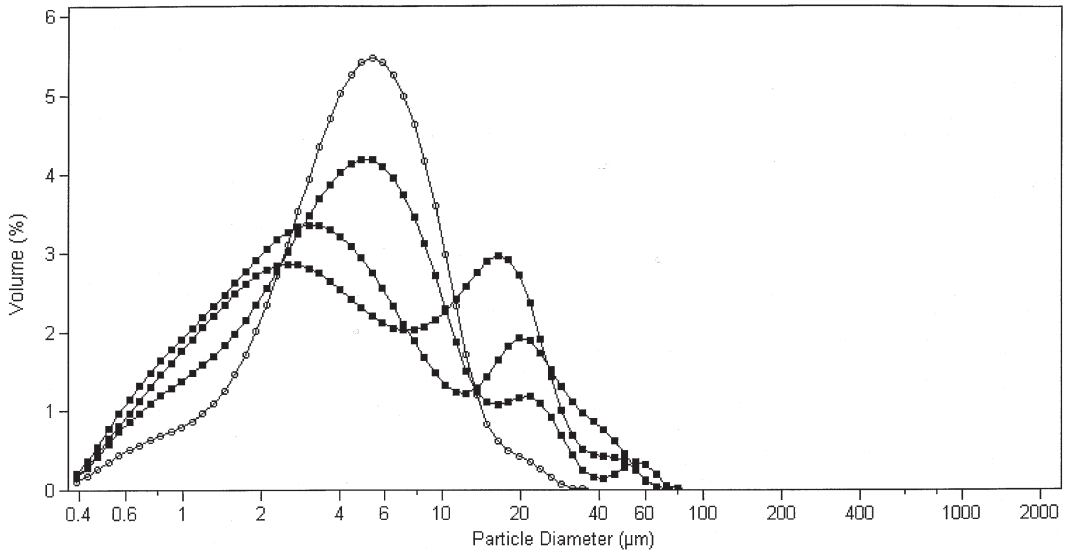

FIG. 8. Particle size distributions from a 10 wt% tripalmitin sample crystallized at 30°C and separated by (A) filtration, ○; (B) centrifugation, ■.

spherulites were only observed under metastable conditions, namely, low supersaturation. Spherulites were not evident in analysis of crystals formed under conditions associated with short induction periods. It should be noted that the samples taken for SEM analysis were not subjected to any mechanical treatment prior to sputtering and observation; the forms indicated are those recovered from the filter surface.

Effect of sample preparation on the crystal size and observed PSD. A comparison was made between the centrifugation and filtration techniques for obtaining samples of crystals. Aliquots (10 mL) of a 10 wt% solution crystallized at 30°C were prepared as described previously. The mass yields of crystals differed by less than 5%, well within experimental error. The samples obtained were compared to investigate possible effects of the preparation method on crystal shape and size.

Figure 8 shows the PSD for the sample prepared by filtration, which is consistent with the results reported above. It also shows some of the PSD obtained *via* the centrifugation technique, clearly revealing bi- or trimodal distributions with a fraction of larger particles in addition to the distribution evident from the sample prepared by filtration. Further sonication (up to 20 min) was performed on the centrifuged samples, but this had no effect on the bimodality or sizes in the distributions. This finding was confirmed by SEM images. Figure 9 shows one such micrograph of a section of a sample separated by centrifugation, showing large platelets interspersed with smaller needle-like crystals, as discussed previously. These results indicate that the centrifugation technique potentially introduces an artifact into the analysis. A possible explanations for the observed differences is that the stress placed on the sample by centrifugation compacts the crystals and induces the formation of large agglomerates. Furthermore, preparation of samples by the centrifugation technique takes significantly longer: 90 min, compared to 5 min using the filtration technique. Moreover, the temperature in the centrifugation step was not controlled and often involved a rise in temperature, which would assist any transformation or crystal growth step. The additional time involved in the preparation routine means that the sample is less likely to be representative of the crystals in solution, as subsequent recrystallization and agglomeration could potentially occur, thus affecting the nature of the crystals formed.

ACKNOWLEDGMENTS

A CASE (Collaborative Awards in Science and Engineering) award for Andrea M. Fitzgerlad from the Biotechnology and Biological Sciences Research Council and United Biscuits, and discussions with Tony Wharton from Beckman Coulter are gratefully acknowledged. The centrifugation studies were performed with the assistance of Felicity Wacher and Isla Harling.

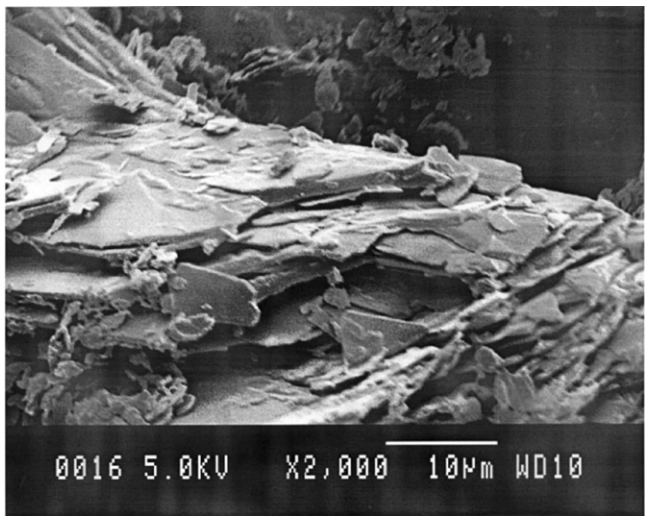

FIG. 9. SEM of 10 wt% tripalmitin sample crystallized at 30°C and separated by centrifugation. For abbreviation see Figure 7.

REFERENCES

1. Ng, W.L., and C.H. Oh, A Kinetic Study of Isothermal Crystallization of Palm Oil by Solid Fat Content Measurements, *J. Am. Oil Chem. Soc. 71*:1135–1139 (1994).
2. Sulaiman, M.Z., N.M. Sulaiman, and S. Kanagaratnam, Triacylglycerols Responsible for the Onset of Nucleation During Clouding of Palm Olein, *Ibid. 74*:1553–1558 (1997).
3. Swe, P.Z., Y.B. Che Man, H.M. Ghazali, and L.S. Wei, Identification of Major Triglycerides Causing the Clouding of Palm Olein, *Ibid. 71*:1141–1144 (1994).
4. Bott, T.R., *Fouling of Heat Exchangers*, Elsevier, Amsterdam, 1995, 546 pp.
5. Hall, J., Computational Fluid Dynamics: A Tool for Hygienic Design, in *Fouling and Cleaning in Food Processing 1998*, edited by D.I. Wilson, P.J. Fryer, and A.P.M. Hasting, No. EUR 18804 (ISBN 92-828-5609-7), Office for Official Publications of the European Communities, Luxembourg, 1999, pp. 144–151.
6. Pan, H.Q., A. Firoozabadi, and P. Fotland, Pressure and Composition Effect on Wax Precipitation: Experimental Data and Model Results, *SPE Production Facilities 12*:250–258 (1997).
7. Majeed, A., B. Bringedal, and S. Overa, Model Calculates Wax Deposition for North Sea Oils, *Oil Gas Jour. 88*:63–69 (1990).
8. Epstein, N., Elements of Particle Deposition onto Nonporous Solid Surfaces Parallel to Suspension Flows, *Exp. Therm. Fluid Sci. 14*:323–334 (1997).
9. Kellens, M., W. Meeussen, and H. Reynaers, Study of the Polymorphism and the Crystallization Kinetics of Tripalmitin: A Microscopic Approach, *J. Am. Oil Chem. Soc. 69*:906–911 (1992).
10. Chawla, P., and J.M. Deman, Measurement of the Size Distribution of Fat Crystals Using a Laser Particle Counter, *Ibid. 67*: 329–332 (1990).
11. Fernandez-Torres, M.J., A.M. Fitzgerald, W.R. Paterson, and D.I. Wilson, A Theoretical Study of Freezing Fouling: Limiting Behavior Based on a Heat and Mass Transfer Analysis, *Chem. Eng. Process. 40*:335–344 (2001).
12. Sato, K., and T. Kuroda, Kinetics of Melt Crystallization and Transformation of Tripalmitin Polymorphs, *J. Am. Oil Chem. Soc. 64*:124–127 *(*1987).
13. Ng, W.L., Nucleation Behavior of Tripalmitin from a Triolein Solution, *Ibid. 66*:1103–1106 (1989).
14. Knoester, M., P. de Bruyne, and M. van den Tempel, Crystallization of Triglycerides at Low Supercooling, *J. Crystal Growth 3*:776–780 (1968).
15. Fitzgerald, A.M., Modelling of Fouling in Food Process Plant, 1998, Certificate of Post-Graduate Study Dissertation, University of Cambridge, 40 pp.
16. Dibildox-Alvarado, E., and J.F. Toro-Vazquez, Evaluation of Tripalmitin Crystallization in Sesame Oil Through a Modified Avrami Equation, *J. Am. Oil Chem. Soc. 75*:73–76 (1998).

[Received March 14, 2001; accepted August 6, 2001]